JTTEE5 16:291–299
DOI: 10.1007/s11666-007-9035-6
1059-9630/$19.00 © ASM International

Effect of Droplet Characteristics and Substrate Surface Topography on the Final Morphology of Plasma-Sprayed Zirconia Single Splats

H.R. Salimijazi, L. Pershin, T.W. Coyle, J. Mostaghimi, S. Chandra, Y.C. Lau, L. Rosenzweig, and E. Moran

(Submitted November 21, 2006; in revised form January 24, 2007)

The morphology of atmospheric plasma-sprayed yttria-stabilized zirconia single splats has been studied. Single splats of plasma-sprayed ZrO_2-7%Y_2O_3 powder have been collected on polished stainless steel substrates kept at three different temperatures (room temperature, 300 °C, and 600 °C). The effect of heating on the substrates' surface topography was evaluated. The effects of spray process parameters such as substrate temperature, particle temperature, and velocity on the morphology of single splats was studied. Variation of splat shape with location within the footprint of plasma spray was investigated. Pore and microcrack formation, splashing behavior, splat/substrate, and splat/splat interfaces were analyzed. Splat morphology and diameter, satellite particles, and splashing behavior were recorded using both scanning electron microscopy and image analysis. Splat/substrate and splat/splat interfaces were studied from cross sections prepared by focused ion beam milling. Results showed primarily disk-shape morphology and no evidence of delamination along the splat/substrate interface at 600 °C substrate temperature. Overlapped splats showed evidence of melting (microwelding) at splat boundaries. Splat thickness was measured to be less than 1 μm for all spray conditions.

Keywords coatings for engine components, influence of process parameters, coatings for gas turbine components, splat morphology, surface and interface characterization

1. Introduction

Yttria-stabilized zirconia plasma spray coatings are widely used for thermal, oxidation, and hot corrosion protection applications in gas turbine and diesel engines. The most common thermal barrier coating material is 7%Y_2O_3-ZrO_2 because of its high temperature phase stability, low thermal diffusivity, and high coefficient of thermal expansion (CTE).

It is known that plasma-sprayed deposits consist of individual splat lamellae formed from molten and resolidified particles which are connected together by mechanical and chemical bonding. Pores are also found at inter-lamellae boundaries, the significance of which depends on the thermal spray process parameters. Thus, the final physical and mechanical properties of such deposits depend on the morphology of individual splats, adhesion between the deposited structure and substrate, cohesive strength within individual splats, the size and morphology of pores, cracks, and defects, and also on the microstructure of the splats themselves (Ref 1-5). It was shown that the in-flight temperature and velocity of the particle upon impact influence the flattening behavior of the splat. The temperature and surface condition of substrates can have a great effect on the final morphology of the splat (Ref 6, 7). It has been observed that increasing substrate temperature reduced the occurrence of splashing and increased the frequency of disk-shape splats. For instance, Jiang et al. (Ref 8) showed that condensates/adsorbates on the substrate surfaces has a significant effect on the splat fragmentation at low substrate temperatures. They found that final splat morphology changes from the splashed/fingered splat to disk-like shape as condensates/adsorbates content on the substrate decreases. Later on, studies by Cedelle et al. (Ref 7) showed that the substrate surface topography is a significant factor on wettability and consequently on the splat formation. They characterized the surface topography of the preheated substrate by a parameter called skewness parameter. This parameter measures the distribution of the surface heights. Their results showed that preheating mirror stainless steel substrates at 400 °C increase the oxide layer thickness and also modifies surface morphology of the substrate in the nanoscale. It promotes wettability and consequently disk-shape splats on the preheated substrates.

However, a pine hole set up to collect single splats on different substrate surfaces was used in the previous

H.R. Salimijazi, L. Pershin, T.W. Coyle, J. Mostaghimi, and **S. Chandra,** Centre for Advanced Coating Technologies, University of Toronto, Toronto, Canada; **Y.C. Lau, L. Rosenzweig,** and **E. Moran,** GE Global Research, Niskayuna, NY, USA. Contact e-mail: jazi@mie.utoronto.ca.

studies (Ref 7-10). Some of them (Ref 8-10) did not measure the particle temperature and velocity upon the impact and if they were measured, they were not incorporated in the final morphology of the splat. The variations of the particle temperature and velocity across the plasma plume were neglected in the previous work. In the current study the effect of substrate temperature on the surface topography of polished stainless steel substrates was studied. Then, the effect of substrate temperature and droplet characteristics, including particle temperature and velocity on the final morphology of single splats of yttria-stabilized zirconia was investigated using a custom-made set up to collect single splats across the plasma plume. The current study attempts to correlate splat shape with the location of the splat within the footprint and the temperature and velocity of droplets in that location, as well as substrate roughness and temperature. Moreover, pore and microcrack formation, splashing behavior, and splat/substrate and splat/splat interfaces were analyzed.

2. Experimental Procedure

This study focuses on the morphology of single splats of thermally sprayed yttria-stabilized zirconia. Single splats of crushed ZrO_2-7%Y_2O_3 powder (Amperit 825-0, −25 μm from H. C. Starck, Germany) have been collected on polished substrates which were kept at three temperatures: room temperature, 300 °C, and 600 °C. The substrates were stainless steel plate, 20 by 20 mm^2 in size and 1.4 mm thick. To narrow the particle size distributions, Amperit 825-0 powders were sieved to −25 μm. Size distributions of powders before and after sieving measured by a particle size analyzer (Mastersizer S from Malvern) are shown in Fig. 1.

To investigate the effect of substrate surface temperature on the polished stainless steel surface topography, substrates were heated to 300 and 600 °C for 15 and 30 min, respectively, kept for 15 min, then air cooled. These heating schedules were similar to the preheating cycles during single-splat collection experiments. Substrate surface morphology of the as-received and preheated substrates was analyzed using a laser confocal microscope (Leica TCS SP2 with a laser system of Ar (50 mW) 458 nm).

Plasma spray experiments were carried out with a SG-100 plasma torch (Praxair, Concord, NH, USA). The plasma torch-substrate distance was maintained at 50 mm during deposition. The typical atmospheric plasma spray parameters and conditions used for collecting single splats are summarized in Table 1.

Particle conditions at the point of impact were monitored by a DPV-2000 system from Tecnar Ltd, Montreal, Canada. The variation in particle conditions through the cross section of the plasma plume was characterized by scanning the cross section of the plume in a 9 by 9 grid with 5 mm steps.

To better correlate varying droplet properties within the plasma plume and final splat morphology, a custom made jig was used to deposit a number of individual splats at different locations within the footprint left by the plasma spray on the substrate. It consists of a sliding shutter with an adjustable slit (see Fig. 2). During spraying the shutter was released and allowed to fall under its own weight, allows a few droplets from each section of the spray to impinge on the substrate as it traversed the plasma spray. The width of the slit was adjusted through trial and error to get the desired density of particles on the substrate, and typically varied from 1 to 2 mm.

Table 1 Atmospheric plasma spray process parameters

Gun	SG 100
Current, A	630
Total gas flow rate, (Ar/He), slpm	50/20
Powder carrier gas (Ar), slpm	9.5
Feed rate, g/min	8
Spray distance, mm	50
Substrate temperature, °C	RT, 300, 600

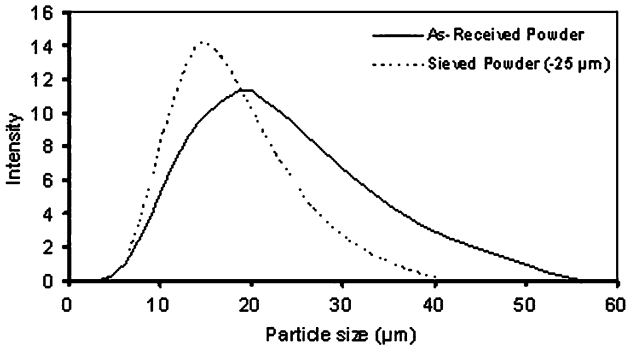

Fig. 1 Particle size distribution of Amperit powders before and after sieving

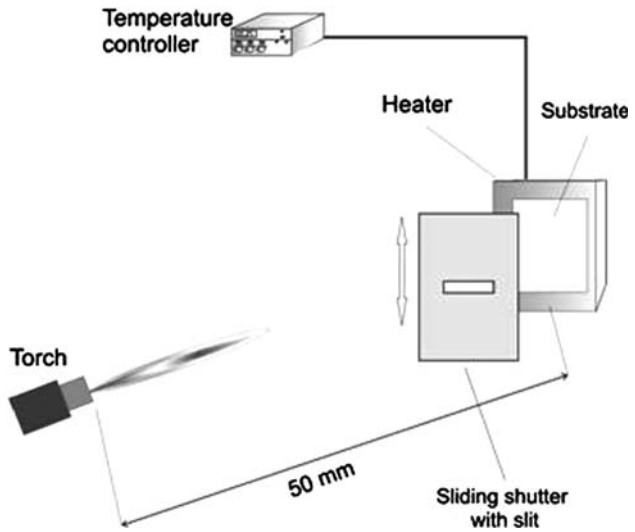

Fig. 2 Experimental setup for single splats deposition in footprint

Splats deposited at various conditions were imaged using scanning electron and optical microscopes. In order to study pore formation, the splat/substrate interface, and the interface between two overlapped splats, cross sections through individual splats were made by Focused Ion Beam (FIB) milling (Micrion Corporation, Peabody, MA). Splat profiles were analyzed with a laser-scanning microscope (VK-8500, Keyence Corp., Osaka, Japan) to characterize the splat morphology.

3. Results and Discussion

3.1 Substrates Surface Analysis

Substrate surface topography of the as-received and preheated polished stainless steel substrates were analyzed by laser confocal microscopy. Figure 3 shows a topographical image of a square 119 by 119 μm region of the polished surface. Roughness was measured along perpendicular line segments in both X and Y directions and also averaged over the entire area shown in Fig. 3. Roughness results are tabulated in Table 2. Higher roughness in the Y direction is due to residual scratching from polishing. The area-averaged roughness was 226 nm.

Figure 4 shows roughness profiles in the X and Y directions. Positions of deep polishing scratches can be seen in the roughness profile in the Y direction, while the surface appears smoother in the X direction.

Figure 5 shows a topographical image of a surface after it was heated to 300 °C and then cooled. The arithmetic roughness in the same direction, parallel to the scratches, was virtually unchanged, going from 226 to 232 nm after heating (Table 2). It is seen that the oxide layer formed on

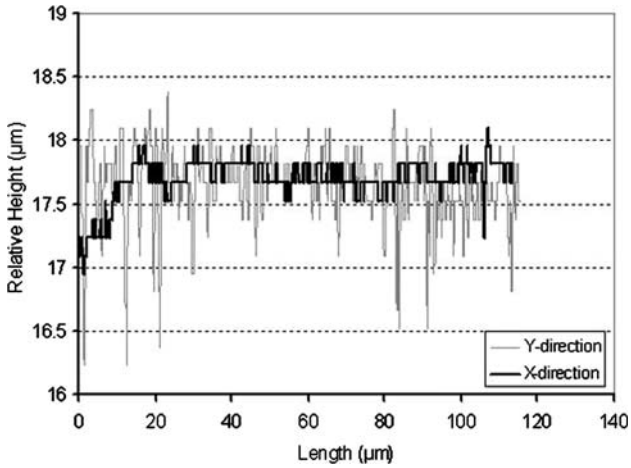

Fig. 4 Roughness profiles of the polished substrate in X and Y directions

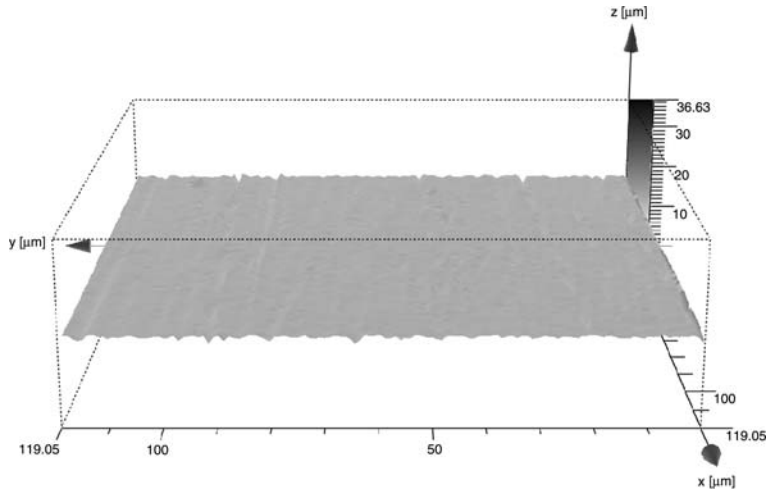

Fig. 3 A topographical image of the polished SS surface

Table 2 Surface roughness measurements data

	Polished SS			Preheated at 300 °C			Preheated at 600 °C		
		Line			Line			Line	
	Region	X	Y	Region	X	Y	Region	X	Y
Area, μm²/Line, μm	11,856	115	113	12,630	111	115	13,448	113	111
Arithmetic average height, roughness, μm	0.19	0.27	0.81	0.232	0.25	0.19	0.84	0.72	0.93
RMS, μm	0.32	0.19	0.15	0.31	0.19	0.15	1.1	0.93	1.2
Min Valley, μm	5.2	1.42	18	4.3	1.14	0.77	6	3.4	3.8
Max. Peak, μm	1.1	0.73	0.44	1.3	0.64	0.34	4.3	2.2	2.5
Average distance, μm	···	~2	~4	···	~3	~2	···	~1	~1.6

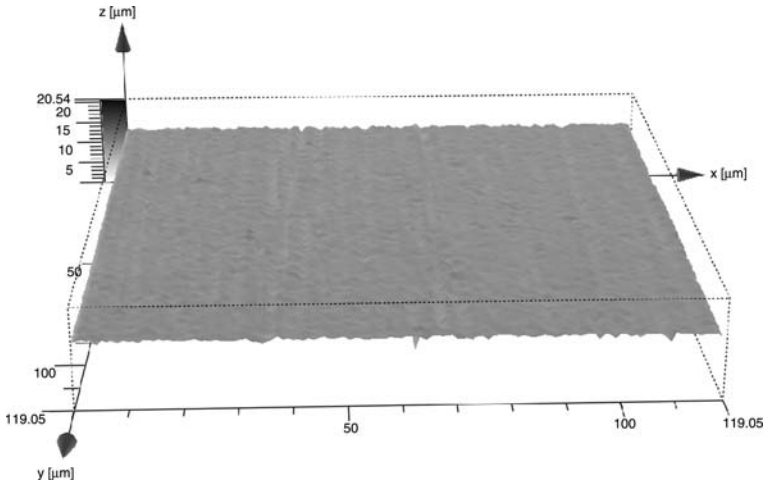

Fig. 5 Topographical image of a preheated polished SS surface at 300 °C

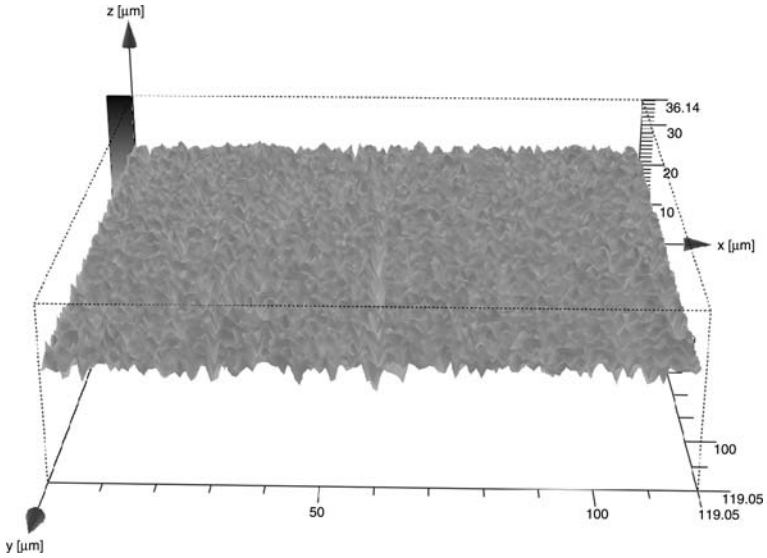

Fig. 6 A topographical image of the preheated substrate at 600 °C

the surface of the substrate changes the surface topography slightly.

Figure 6 shows an image of the surface topography of the specimen preheated at 600 °C and then cooled. Surface topography changed significantly compared to the polished samples and even preheated samples at 300 °C. Roughness measurements within the area of interest give an arithmetic average roughness of 0.84 µm. Roughness in both X and Y directions are almost the same with a step height of around 1-1.6 µm. Surface characteristics of the preheated substrates are summarized in Table 2. Roughness profiles of the polished and preheated surfaces along a line segment in the same direction are shown in Fig. 7. While the frequency of heights does not change, amplitude of bumps in the oxidized surfaces at 600 °C increases significantly.

3.2 Single-Splats Analyses

Results of the DPV-2000 scan for droplet temperature and velocity distributions at impact are presented in Fig. 8. Initially the DPV sensor was aligned with the centerline of the torch. The average particle temperature and velocity at the center of the plume were measured from 2470 particles and were $T = 2836 \pm 166$ °C and $V = 307 \pm 74$ m/s, respectively. The position of the plasma gun nozzle is marked with a dashed circle in the figure.

Figure 9 shows a montage of optical images from the upper portion of the footprint obtained using the custom-made shutter rig set up. The marked oval represents the deposition area or footprint across the plasma plume, showing a variation in splat density from the center to the periphery of the footprint. The substrate temperature was

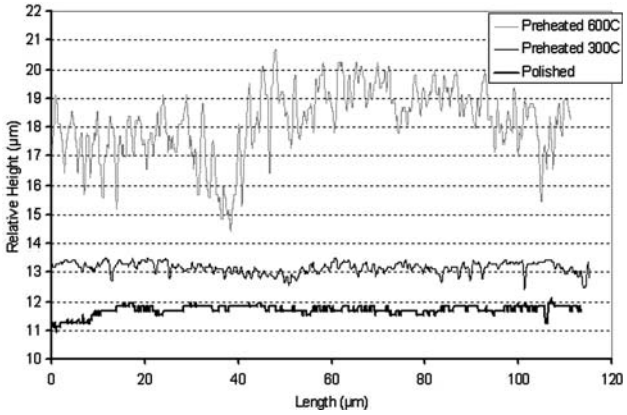

Fig. 7 Roughness profiles of the polished and preheated substrates in the same direction

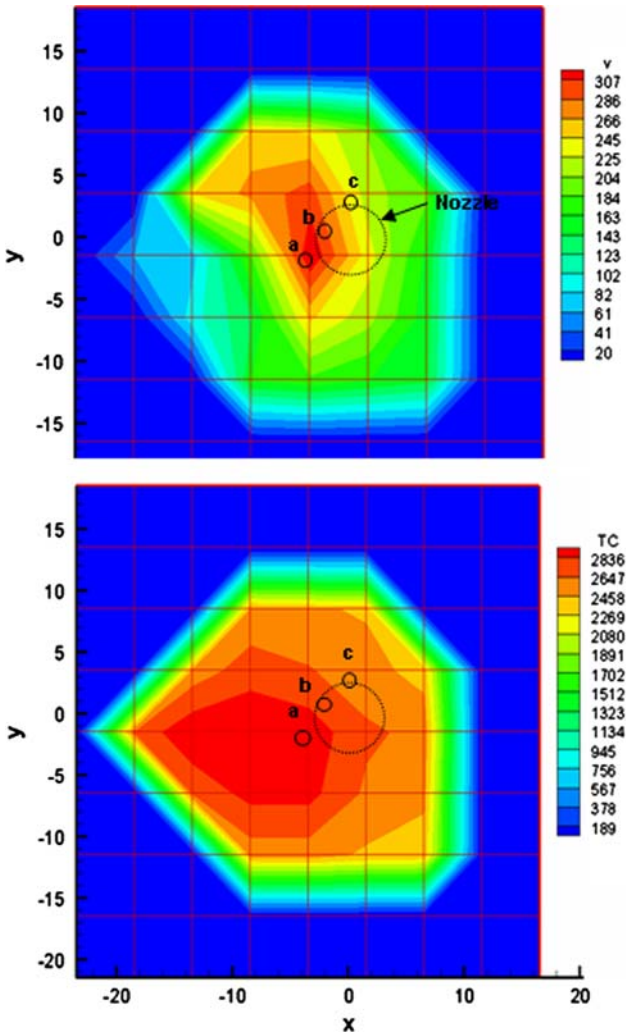

Fig. 8 DPV scan of the plasma plume from Amperit 825-0 powder at 50 mm spray distance. Micrographs from locations (a), (b), and (c) are shown in Fig. 9-11

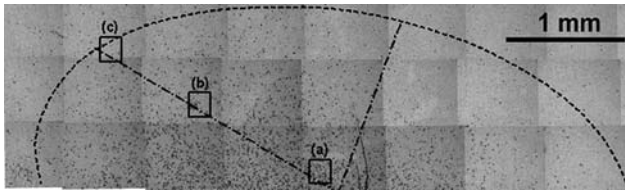

Fig. 9 Upper part of the footprint obtained by the shutter

initially kept at 300 °C in this picture. No complete single splats were collected on the substrate, which was kept initially at room temperature, due to extensive splashing and fragmentation of the impacting molten particles. Only a portion of the central part of the splats remained on the surface while the rest of the splat spalled from the surface. It has been shown that the flatting behavior of the splat and splat/substrate adhesion depends strongly on the adsorbates and condensates on the unheated surface of the substrate on which plasma-sprayed particles impact (Ref 6, 8, 11, 12). The linkage between the adsorbates/condensates and final splat morphology was explained by Jiang et al. (Ref 8). They can form a gaseous pore trapped within the splat/substrate interface due to condensate vaporization. Then, the trapped gas acts as a thermal barrier between the substrate and splat resulting in increased thermal contact resistance, reduced cooling rate of particles, and finally flow instability-induced splashing. The pores formed in the interface also reduce the droplet adhesion.

Splats collected on the polished substrate held at 300 °C from three areas within the footprint are shown in Fig. 10. The locations of the micrographs within the footprint are shown with the marked squares in Fig. 9 and the corresponding locations within the plasma plume are shown in Fig. 8. As we move from the center to outwards in the footprint, the number of splats was reduced, the average temperature and velocity of the particles is reduced, and the fraction of splats which were splashed and fragmented increased. No complete single splats were collected on the periphery of the footprint because particle temperatures were very close to or below the melting point of zirconia. In this condition, almost all particles impacted on the periphery of the footprint were bounced from the surface and only some debris remained. The in-flight particle temperature was improved as we move towards the center of the plasma plume as it can be seen in Fig. 8. The single splats at the center of footprint, Fig. 10(a), show finger formation and splashing clearly. Since no significant differences in the topography of the substrate surface kept at room temperature and 300 °C have been observed, the large differences observed in the final splat morphology when the substrate is heated to 300 °C are probably because of the removal of condensates and adsorbates on the surface of the substrate, resulting in reduced thermal contact resistance. It can be observed from the single splats density in the footprint deposited at room temperature and 300 °C that while splats collected on the unheated substrates are loosely

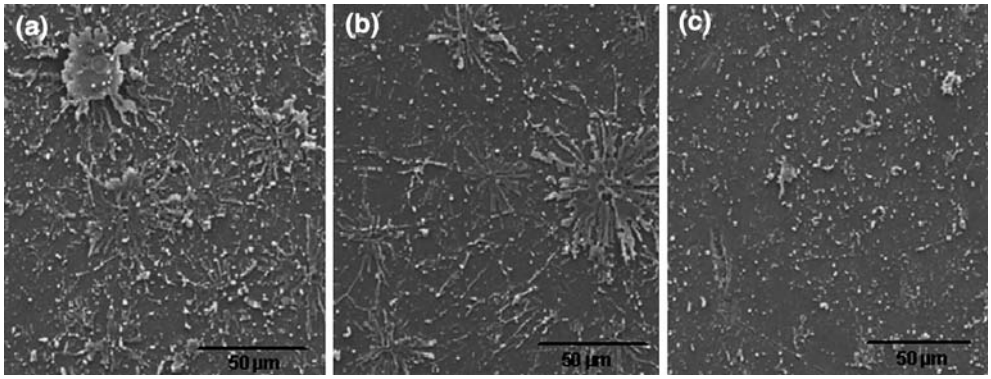

Fig. 10 Single splats morphology of as-received Amperit 825-0 particles deposited at 50 mm spray distance and 300 °C substrate temperature

adhered to the surface and lost during handling, the splats prepared on the preheated substrate can remain attached during analyses. Increasing the adhesion of splats by removing the condensate and adsorbates has also been reported by Jiang and Sampath (Ref 8, 9).

For a single splats deposited on a substrate held at 600 °C (Fig. 11), it was observed that almost 90% of the collected single splats have a pancake shape with a lower fraction of splashed and fragmented particles and fingers compared to the colder substrates. The formation of disk-like splats could be attributed to a change in substrate surface topography. Significant increases in the height of the surface asperities and heights distribution can be seen for the substrate heated at 600 °C as shown in Fig. 6 and 7. Such changes in surface topology could alter the wetting behavior and the thermal contact resistance between the splat and substrate, thereby affecting the spreading and solidification dynamics. Cedelle et al. (Ref 7) shown that the static and dynamic wettability of molten drops improve by preheating substrates. Increasing the substrate surface wettability can reduce the spreading time and increase the cooling rate of the splats, resulting in disk-shape splats collected on the preheated substrate at 600 °C. The number of satellite droplets increased for particles which impacted on the periphery of the footprint. Some partially molten particles were observed in the periphery of the footprint due to the low temperature of the particles. Compared to the splats deposited on the preheated substrate at 300 °C, the density of single splats in the preheated substrate at 600 °C increased significantly. It can be concluded that the splats adhesion in the latter case is higher due to increasing the roughness surface and therefore the real contact area between the substrate and splats. Some disk-shape splats can be observed even in the periphery of the footprint, indicating improvement of the wettability of the surface of the preheated substrates.

To study the splat-substrate interface, splat curl up, and the interface between overlapped splats, splat cross sections were made using the FIB milling technique. FIB systems use a finely focused beam of gallium ions that can be operated at low-beam currents for imaging or high-beam currents for site-specific sputtering or milling. The FIB microscope can be used as an atomic scale-milling machine to perform stress-free precision sectioning with sub-micron positional accuracy instead of using conventionally metallographic procedures which may introduce artifacts and residual stresses.

The micrographs in Fig. 12 show top and cross sectional views of splats deposited on a polished substrate initially at 300 °C. Finger formation and splashed particles can be clearly observed. It appears that the splat at the bottom of Fig. 12(a) was a partially molten particle at the point of impact. Black lines marked in Fig. 12(a) show the position of the section made by ion milling. Figure 12(b) shows the cross section of the edge of the splat, where splat curl up can be observed. Figure 12(c) shows the cross sectional view of the overlapped area marked by a back line in Fig 12(a). Columnar grains are revealed within the splats in Fig. 12(b) and (c) after etching the cross section with gallium ions. Columnar grains at the edge of the splat, where the splat has curled up, are perpendicular to the substrate indicating that the splat separated from the substrate after solidification. In Fig. 12(c) fine pores can be seen along the boundary between splats. However, the columnar structure is continuous across this boundary. A region of noncolumnar structure can be seen above the overlapped region. The cooling rate and temperature gradient may have been lower at this location giving rise to an equiaxed grain structure as observed by Chraska et al. (Ref 10).

Vertical cracks in the cross section of YSZ single splats can be observed. These cracks form after solidification due to the thermal contraction during cooling. If the splat adheres well with the substrate, the cracks relax the in-plane quenching stresses (Ref 10). Since almost each vertical crack is associated with a horizontal crack at the splat/substrate interface, some limited displacement of the coating fragments along the microcracks can be observed.

Figure 13 shows two overlapping splats deposited on the polished stainless steel substrate initially held at 300 °C. A partially molten splat can also be observed in the bottom right corner of the micrograph. A cross section along the line drawn in Fig. 13(a) is shown in Fig. 13(b). It

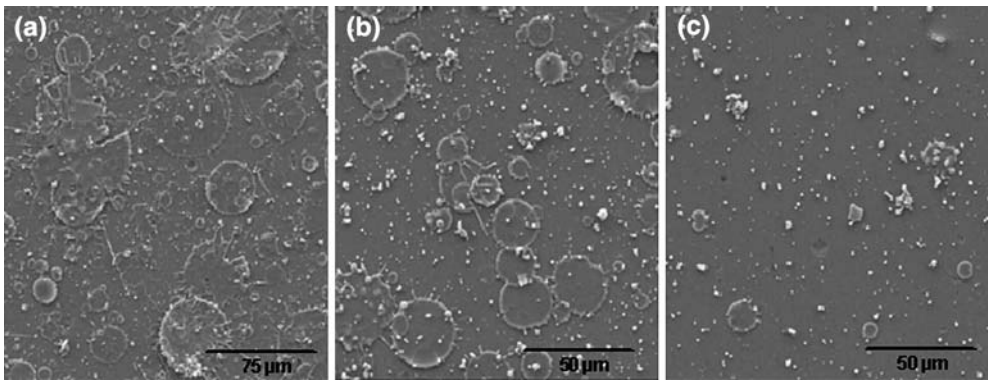

Fig. 11 Single splats morphology of as-received Amperit 825-0 deposited at 50 mm spray distance and 600 °C substrate temperature

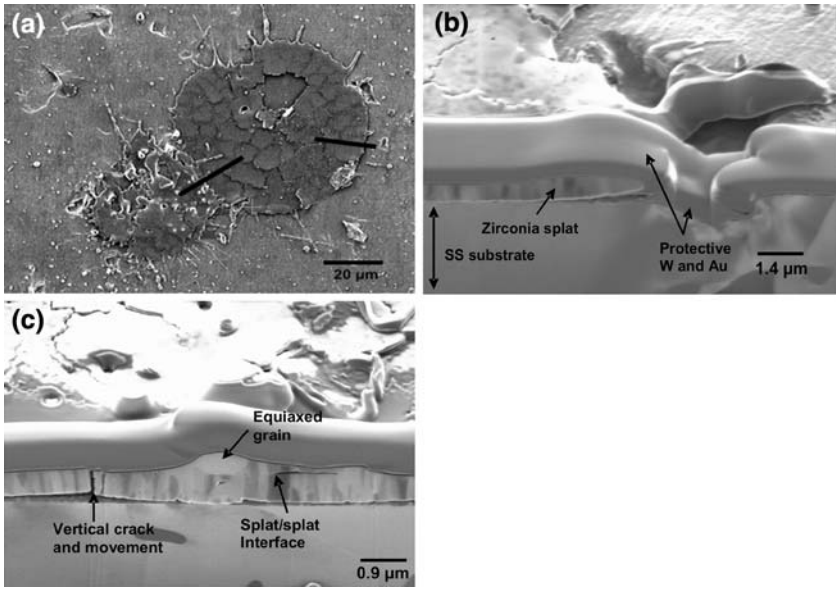

Fig. 12 SEM micrographs obtained from FIB microscope showing (a) top view of two splats, (b) cross section of the splat at the edge, marked in Fig. 12(a) and (c) cross section of the overlapped area marked in Fig. 12(a)

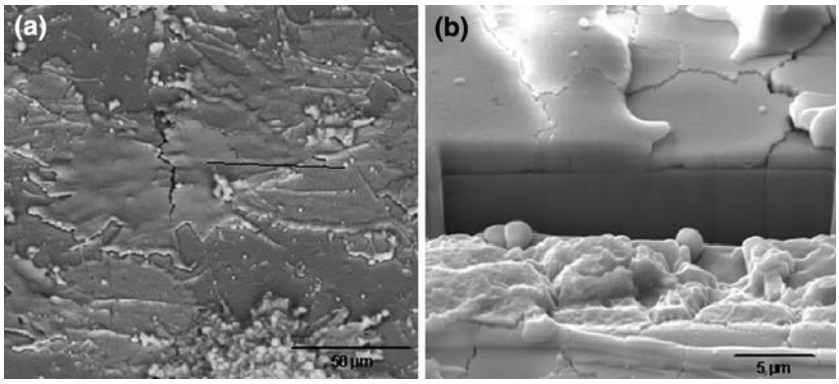

Fig. 13 SEM microimages of (a) top view of two overlapped splats and (b) cross section of the overlapped area marked in Fig. 13(a)

shows better contact between the splats and substrate compared to the previous overlapped splats shown in Fig. 12. There is no visible interface between the splats on the cross section, Fig. 13(b). Microcracks can be seen within the splats due to stresses induced during and after solidification.

Figure 14 shows overlapping splats, one completely and the other partially melted, deposited at the 50 mm spray distance on a polished stainless steel substrate initially kept at 600 °C. There is no evidence of the splat/splat interface in the cross section of the overlapped splats (Fig. 14c), indicating good contact along the interface of the overlapping splats. Through-thickness microcracks are seen in areas where there is good contact between the splat and the substrate. However, near the edge of the splat, where no microcracking is evident, residual stresses were relaxed by curl up (Fig. 14d). Figure 14(d) also shows a region of very fine equiaxed grains close to the interface and the jetting of the molten material out over the previously solidified layer (fine grain structure) at the periphery of the flattened splat during spreading. This phenomenon has been shown in numerical simulations (Ref 13, 14), where radially flowing liquid jets over a solidified rim, disintegrated to form fingers and satellite droplets.

Image analysis was performed in order to determine the average splat diameter, number of fingers, and the average size of splashed particles and fingers. Results obtained from different spray conditions are tabulated in Table 3. The results were obtained from analyzing more than five splats randomly selected on the surface of the substrate, close to the center of the footprint, for each condition. In this region of the footprint, in-flight particles have maximum velocity and temperature at the point of impact compared to the periphery of the footprint. The average splat diameter was much smaller for room temperature substrates than for 300 °C and 600 °C substrates because only a portion of the central part of the splats

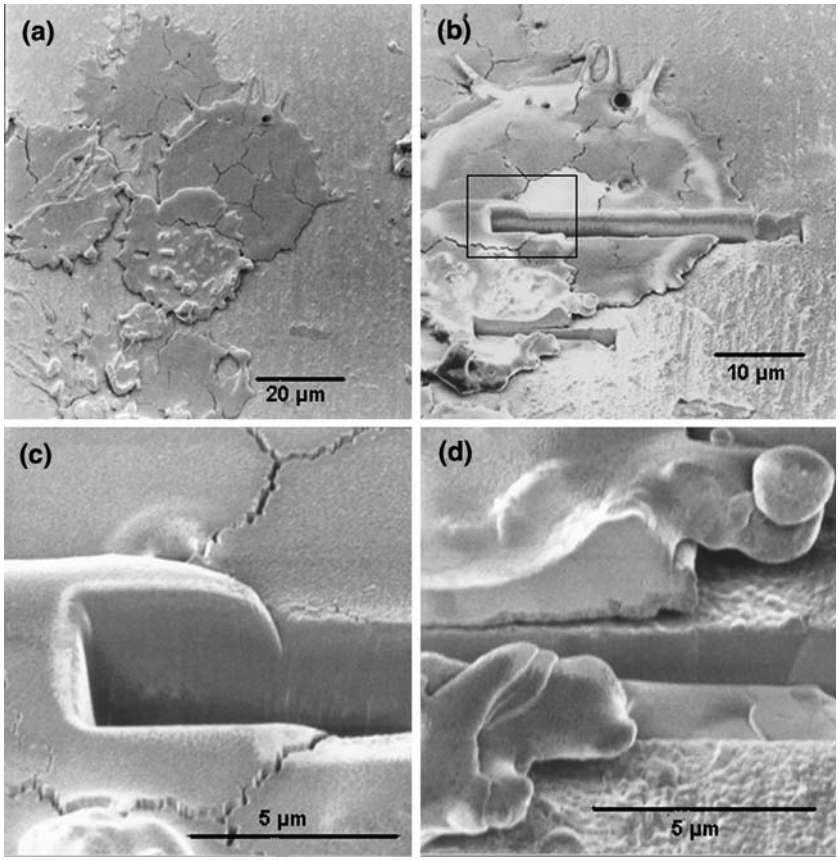

Fig. 14 Cross section of single splats deposited on the polished SS substrate initially kept at 600 °C. (a) and (b): Top view of a partially melted splat overlapping a completely melted splat; (c) Overlapped interface of the rectangle shown in Fig. 14(b); and (d) curl up at the edge of a partially melted splat

Table 3 Image analysis data obtained from different spray conditions

Conditions temperature, spray distance	Average splat diameter, μm	Average satellite diameter, μm	Number of fingers	Average length of fingers, μm	Average width of fingers, μm	Volume fraction of splat	Volume fraction of satellites
Room temperature, 50 mm	15±3	0.3±0.2	29±6	6±0.3	1.4±0.4	84±8%	16±5%
300 °C, 50 mm	53±2	0.4±0.3	51±18	11±5	1.4±0.3	91.3±0.5%	9±1%
600 °C, 50 mm	46±0.1	0.6±0.4	65±8	7.1±0.4	1±0.25	93±5%	6±3%

remained on the surface while the rest of the splat spalled off the substrate. The average diameter of the satellite droplets was around 0.5 μm. The volume fraction of the main splats compared to the volume fraction of the satellite particles was increased by increasing the substrate temperature, indicating less splashing and good wettability and contact at higher substrate temperature.

4. Conclusion

In the present research, the final morphology of single splats of yttria partially stabilized zirconia was correlated with the location of the splat within the plasma plume and the temperature and velocity of droplets in that location, as well as substrate surface condition and temperature. Results indicate that not only the substrate roughness and temperature play a critical role in the splat formation but also in-flight particle temperature and velocity at the point of impact have a significant effect on the final morphology of the splat. Particles that impacted on substrates initially kept at room temperature were splashed, disintegrated to form fragmented particles, and finally detached from the surface. This scenario is worse when particles impacted on the periphery of the footprint. It indicates that both adsorbates on the surface and low droplet temperature in the periphery play role in the flattening behavior of the splat. Droplets that impacted substrates preheated to 300 or 600 °C showed reduced disintegration and higher adhesion compared to the particles that impacted on the substrates kept at room temperature. This suggests that the contact between the splat and substrate is better, probably due to desorption of adsorbates and condensates on the surface. The disk-like shape splat and good splat/substrate adhesion on the substrates preheated to 600 °C, compared to particles that impacted on the cooler substrates, indicates that the increased roughness and changes in the surface topography observed under these conditions significantly improved wettability and solidification behavior. Particles in the periphery of the plasma plume which impacted far from the center of the footprint exhibited more splashing and fragmented particles compared to those impacted on the center of the footprint regardless of substrate temperature. Splat curl up was found along the periphery of the splats due to shrinkage during cooling from the solidification temperature. A high density of microcrack networks can be observed on splats which are in good contact with the substrate, also attributed to the stresses arising during cooling down from the melting point to the substrate temperature.

References

1. A. Kucuk, C.C. Berndt, U. Senturk, R.S. Lima, and C.R.C. Lima, Influence of Plasma Spray Parameters on Mechanical Properties of Yttria Stabilized Zirconia Coatings. I: Four Point Bend Test, *Mater. Sci. Eng.*, 2000, **A285**, p 29-40
2. G. Antou, F. Hlawka, G. Montavon, C. Coddet, A. Cornet, and F. Machi, Thermal Behavior of Y-PSZ TBCs In Situ Remelted During their Deposition, *International Thermal Spray Conference, Thermal Spray Connects: Explore its Surfacing Potential*, E. Lugscheider, Ed., May 2-4, 2005 (Basel, Switzerland), ASM International, 2005
3. W.-Z. Wang, C.-J. Li, and K. Sonoya, Study of Lamellar Microstructure of Plasma-Sprayed ZrO2–8 wt.%Y2O3 Coatings, *International Thermal Spray Conference, Thermal Spray Connects: Explore its Surfacing Potential*, E. Lugscheider, Ed., May 2-4, 2005 (Basel, Switzerland), ASM International, 2005
4. H.R. Salimijazi, T.W. Coyle, J. Mostaghimi, and L. Leblanc, Microstructure of Vacuum Plasma-Sprayed Boron Carbide, *J. Therm. Spray Technol.*, 2005, **14**(3), p 362-368
5. G. Montavon, S. Sampath, C.C. Berndt, H. Herman, and C. Coddet, Effect of Vacuum Plasma Spray Processing Parameters on Splat Morphology, *J. Therm. Spray Technol.*, 1995, **4**(1), p 67-74
6. A. McDonald, M. Lamontagne, S. Chandra, and C. Moreau, Photographing Impact of Plasma-Sprayed Particles on Metal Substrates, *Proceeding of the 2006 international Thermal Spray Conference*, B. Marple, M. Hyland, Y.C. Lau, R.S. Lima and J. Voyer, Eds., May 15-18 (Seattle, WA), 2006
7. J. Cedelle, M. Vardelle, and P. Fauchais, Influence of Stainless Steel Substrate Preheating on Surface Topography and on Milimeter- and Micrometer-Sized Splat Formation, *Surf. Coat. Technol.*, 2006, **201**, p 1373-1382
8. X. Jiang, Y. Wan, H. Herman, and S. Sampath, Role of Condensates and Adsorbates on Substrate Surface on Fragmentation of Impinging Molten Droplets During Thermal Spray, *Thin Solid Film*, 2001, **385**, p 132-141
9. S. Sampath, X.Y. Jiang, J. Matejicek, A.C. Leger, and A. Vardelle, Substrate Temperature Effects on Splat Formation, Microstructure Development and Properties of Plasma Sprayed Coatings Part I: Case Study for Partially Stabilized Zirconia, *Mater. Sci. Technol.*, 1999, **A272**, p 181-188
10. T. Chraska and A.H. King, Effect of Different Substrate Conditions Upon Interface with Plasma Sprayed – A TEM Study, *Surf. Coat. Technol.*, 2002, **157**, p 238-246
11. M. Fukumoto, H. Nagai, and T. Yasui, Influence of Surface Character Change of Substrate due to Heating on Flattening Behavior of Thermal Sprayed Particle, *Proceeding of the 2006 International Thermal Spray Conference*, B. Marple, M. Hyland, Y.C. Lau, R.S. Lima and J. Voyer, Eds., May 15-18 (Seattle, WA), 2006
12. A. McDonald, M. Lamontagne, S. Chandra, and C. Moreau, Photographing Impact of Plasma-Sprayed Zirconia and Amorphous Steel Particles on Hot and Cold Glass Substrate, *Proceeding of the 17th International Symposium on Plasma Chemistry*, J. Mostaghimi, H.R. Salimi Jazi, V. Pershin and T. Coyle, Eds., Aug. 7-12 (Toronto, Canada), 2005
13. M. Pasandideh-Fard, R. Bhole, S. Chandra, and J. Mostaghimi, Deposition of Tin Droplets on Steel Plate: Simulations and Experiments, *Int. J. Heat Mass Transfer*, 1998, **41**, p 2929-2945
14. M. Pasandideh-Fard, V. Pershin, S. Chandra, and J. Mostaghimi, Splat Shape in a Thermal Spray Coating Process: Simulations and Experiments, *J. Thermal Spray Technol.*, 2002, **11**(2), p 206-217